Selective Laser-Assisted Synthesis of Tubular van der Waals Heterostructures of Single-Layered PbI_2 within Carbon Nanotubes Exhibiting Carrier Photogeneration

Stefania Sandoval,[‡] Dejan Kepić,[‡,†] Ángel Pérez del Pino,[,‡] Enikö György,[‡] Andrés Gómez,[‡] Martin Pfannmoeller,[§] Gustaaf Van Tendeloo,[§] Belén Ballesteros[*,ǁ] and Gerard Tobias[*,‡]*

[‡]Institut de Ciència de Materials de Barcelona (ICMAB-CSIC), Campus UAB, Bellaterra, 08193 Barcelona, Spain

[†]Vinča Institute of Nuclear Sciences, P.O. Box 522, University of Belgrade, 11001 Belgrade, Serbia

[§]Electron Microscopy for Materials Research (EMAT), University of Antwerp, Groenenborgerlaan 171, 2020 Antwerp, Belgium

[ǁ]Catalan Institute of Nanoscience and Nanotechnology (ICN2), CSIC and The Barcelona Institute of Science and Technology, Campus UAB, Bellaterra, 08193 Barcelona, Spain

*Corresponding authors E-mail: gerard.tobias@icmab.es, aperez@icmab.es; belen.ballesteros@icn2.cat

ABSTRACT: The electronic and optical properties of two-dimensional layered materials allow the miniaturization of nanoelectronic and optoelectronic devices in a competitive manner. Even larger opportunities arise when two or more layers of different materials are combined. Here we report on an ultrafast energy efficient strategy, using laser irradiation, which allows bulk synthesis of crystalline single-layered lead iodide in the cavities of carbon nanotubes by forming cylindrical van der Waals heterostructures. In contrast to the filling of van der Waals solids into carbon nanotubes by conventional thermal annealing, which favors de formation of inorganic nanowires, the present strategy is highly selective towards the growth of monolayers forming lead iodide nanotubes. The irradiated bulk material bearing the nanotubes reveals a decrease of the resistivity as well as a significant increase in the current flow upon illumination. Both effects are attributed to the presence of single-walled lead iodide nanotubes in the cavities of carbon nanotubes, which dominate the properties of the whole matrix. The present study brings in a simple, ultrafast and energy efficient strategy for the tailored synthesis of rolled-up single-layers of lead iodide (*i.e.* single-walled PbI_2 nanotubes), which we believe could be expanded to other two-dimensional (2D) van der Waals solids. In fact, initial tests with ZnI_2 already reveal the formation of single-walled ZnI_2 nanotubes, thus proving the versatility of the approach.

KEYWORDS: 2D materials, lead iodide, zinc iodide, metal halides, single-walled inorganic nanotubes, core-shell, encapsulation

Two-dimensional layered materials have become a major focus of research because of their extraordinary properties.[1-4] The high flexibility of single-layered crystals allows rolling them up to form tubular structures which combine the properties of both two-dimensional and one-dimensional materials, further expanding their range of application.[5] Strain engineering can be accomplished by bending two-dimensional materials allowing a fine tuning of their properties.[6] For example, rolling up MoS_2 sheets induces a tunable semiconducting to metallic phase transition,[7] and an enhanced photoabsorption when integrated into rolled-up heterostructures compared to their "flat" configuration.[8] Scrolled graphene/polycarbonate fibers show exotic telescoping elongation at break 30 times greater than Kevlar.[9] Apart from nanoscrolls, cylindrical two-dimensional materials (*i.e.* nanotubes) are formed when two parallel edges are seamlessly joined. Edge states have a strong effect on the electronic properties of two-dimensional materials.[10] Cylindrical 2D materials are being explored for nanophotonic circuitry because compressing and channeling of plasmons suffer from scattering at the edges of 2D sheets.[11] From just these few examples it is clear that single-layered nanotubes, commonly referred to as single-walled nanotubes, are of great interest for technological applications. However, despite efforts on the synthesis of nanotubes started more than a decade before the interest on their two-dimensional “flat” analogues, the amount of single-walled inorganic nanotubes reported to date is limited because their multi-walled counter parts are favored during synthesis.[12] The synthesis of elusive single-walled inorganic nanotubes remains as a grand challenge.[13] Therefore, strategies are needed to fill this gap. A variety of single-walled nanotubes with a high catalytic performance,[14, 15] not restricted to layered structures in their bulk form, have recently been synthesized taking advantage of weak interactions between building blocks.[14-16] When it comes to the synthesis of single-walled nanotubes of van der Waals solids, which are the scope of the

present study, we recently reported on the use of carbon nanotubes for the template directed growth of single-walled materials in their interior.[17] The synthetic strategy proved to be versatile but requires the use of high temperatures for prolonged periods of time. Furthermore, even under the best synthetic conditions, a large fraction (at least 35 %) of other nanostructures are formed in the interior of the carbon nanotubes[18] which could strongly influence the properties. Here we present an ultrafast, energy efficient and easily scalable approach that allows the selective synthesis of single-walled lead iodide nanotubes coating the inner walls of carbon nanotubes, thus forming cylindrical van der Waals heterostructures. By exploiting the properties of van der Waals heterostructures, a variety of designs and devices emerge.[19, 20] For instance, the combination of graphene with light-sensitive materials allows the creation of efficient photodetectors[21] and photoresponsive memory devices.[22] We focused the present study on the growth of monolayers of lead iodide since this material is of interest not only as a room-temperature detector of γ- and X-radiation[23] but has also become a strategic material for hybrid solar cells.[24] Actually, interfacing electrically active graphene with light sensitive lead iodide has been predicted to substantially enhance its visible light response.[25] To complete the study, the optoelectronic properties of the resulting heterostructures embedded in the bulk matrix of lead iodide have been investigated. Remarkably, whereas lead iodide monolayers must be handled under inert atmosphere to avoid decomposition,[26] the composite materials prepared here can be handled in air since the carbon shell offers protection to the lead iodide single-layers.

RESULTS AND DISCUSSION

Laser-Assisted Filling of Carbon Nanotubes. The encapsulation of materials into the cavities of previously synthesized carbon nanotubes (CNTs) requires that the filling material either melts

or sublimes to allow its incorporation when using high temperature filling strategies.[27-30] Alternatively, solution filling can be employed but lower filling yields are generally reported and further processing is required to eliminate the solvent, unless the solvent itself is the chosen material.[31-34] The controlled synthesis of materials within the cavities of CNTs is getting an increased attention,[35-37] and for instance MoS_2 and WS_2 nanoribbons have been prepared in this manner.[27, 38] Laser irradiation of materials can lead to a fast and local increase of the temperature and arises as a promising alternative to the conventional annealing using furnaces that have been widely employed to achieve molten phase capillary filling.[39-41] Lead iodide single-walled nanotubes were grown by laser irradiation of a pellet consisting of open-ended multi-walled carbon nanotubes (MWCNTs) finely mixed with lead iodide powder. A schematic representation of the employed process is shown in Figure 1A. Pellets of 1.3 cm in diameter and ca. 0.5 mm in thickness were prepared by applying a pressure of 10 T to the MWCNT/PbI_2 mixture. A variety of incident laser fluences (40-100 $mJ \cdot cm^{-2}$) was employed using different number of pulses (10, 100 and 1000 pulses per site). Photothermal simulations were initially performed to obtain information about the temporal evolution of the temperature reached by the target during the irradiation with different laser fluences in the 40-100 $mJ \cdot cm^{-2}$ range. An idealized system, composed of a MWCNT immersed in a PbI_2 matrix was employed. Figure 1B shows that the melting temperature of PbI_2 (Tm = 410 ºC,[42] purple dashed line) would be already exceeded even at the lowest considered laser fluence (530 °C, 40 $mJ \cdot cm^{-2}$), exhibiting extremely high heating-cooling rates (up to ca. 2×10^9 $°C \cdot s^{-1}$). In these conditions, the maximum temperature is close to the temperature previously employed for the synthesis of PbI_2 nanotubes by conventional annealing treatments (500 °C).[17] The peak temperature is reached at about 4 ns and increases

with the applied laser fluence. The maximum achieved temperature with the current strategy would be ca. 950 °C, after irradiation at 100 $mJ \cdot cm^{-2}$.

Structural Analysis of Cylindrical van der Waals Heterostructures. Analyses of the laser irradiated samples by back-scattered scanning electron microscopy (SEM), which provides Z-contrast images of the samples, indicated that filling of the CNTs occurred in the whole range of laser fluences and number of accumulated pulses (Figure S1). A small fraction of the pellet irradiated at different laser fluences and pulses was gently scratched and characterized by high-angle annular dark field (HAADF) imaging in high resolution scanning transmission electron microscopy (STEM). Regardless of the laser fluence (40-100 $mJ \cdot cm^{-2}$) and pulses employed (10, 100 and 1000 pulses) the vast majority of MWCNTs that were filled with PbI_2 presented the characteristic contrast of PbI_2 nanotubes and a minority of them revealed the presence of PbI_2 nanowires. A representative HAADF-STEM image providing a general view of the sample prepared at 80 $mJ \cdot cm^{-2}$ fluence and 1000 pulses is presented in Figure 2A and additional images are included in Figure S2. Since HAADF-STEM imaging is strongly dependent on the atomic number Z,[43] heavy elements such as Pb (Z = 82) and I (Z = 53) appear with a bright contrast, whereas carbon (Z = 6) appears as pale grey. As it can be seen in the images, the inner cavities of the hosting CNTs are contoured by bright lines indicating the successful formation of single-walled PbI_2 nanotubes in their interior. At low laser fluences the observed inorganic PbI_2 presented a more defective/fractioned structure than at higher fluences. Figure S3 shows HAADF-STEM images of the sample prepared at 40 $mJ \cdot cm^{-2}$ fluence and 1000 pulses. Visual inspection of the irradiated pellet already reflects the cumulative effect of increasing the number of laser pulses (Figure S4). Thus, the highest amount of PbI_2 filled MWCNTs would be expected at 1000 pulses. A quantitative determination of the ratio between filled and empty MWCNTs is

not possible since the irradiated areas were manually scratched for HAADF-STEM inspection. During this process non-irradiated areas could be also collected and imaged.

It is worth stressing that all the inorganic PbI_2 nanotubes imaged in the present study (over 1000) are single-walled. The presence of multi-walled PbI_2 was not observed regardless of the laser fluence and pulses employed. Two additional samples were prepared to assess whether the use of higher fluence (200 $mJ \cdot cm^{-2}$, 1000 pulses) or number of pulses (10000 pulses, 100 $mJ \cdot cm^{-2}$) would favor the formation of multi-walled PbI_2. Despite the extremely high temperature developed in the material at 200 $mJ \cdot cm^{-2}$ (ca. 1700 °C according to simulation, Figure S5) and much longer irradiation time, analyses of the irradiated areas by HAADF-STEM revealed the absence of multi-walled nanotubes.

We also investigated the stability of the confined monolayers one year after their synthesis. Samples were kept under ambient conditions, thus exposed to humidity and air. Despite PbI_2 is a rather unstable material which can decompose gradually in wet air,[26] HAADF-STEM imaging reveals the presence of PbI_2 nanotubes still inside the cavities of CNTs with only partial damage in some areas (Figure S6; 80 $mJ \cdot cm^{-2}$ fluence and 1000 pulses). This microscopy analysis confirms that MWCNTs not only act as templates for the growth of tubular inorganic nanostructures, but also offer shielding and protection of the inner PbI_2 nanotubes from the external environment. This is a major advantage compared to physical vapor deposition grown PbI_2 layers were the synthetic process, conservation, and testing has to be carried out under an inert atmosphere (N_2) or under vacuum conditions.[26] Further analysis with a state-of-the-art aberration corrected electron microscope was performed on the one year old sample to confirm the presence of PbI_2 monolayers. Figure 2B shows a high resolution HAADF-STEM image of an individual PbI_2 nanotube confined within a MWCNT. Due to the tubular nature of the material,

brighter lines are observed at the edges indicating a higher density of atoms in the projected image, while the central area presents a lower contrast due to the presence of a hollow cavity. The PbI_2 nanotube wall thickness (ca. 0.4 nm), indicated in the figure by orange lines, is in agreement with that of an individual layer of PbI_2.[44] Both the curvature and the crystallinity of the structure are well appreciated.

In order to provide direct evidence of the superiority of the laser-assisted approach compared to the conventional thermal annealing treatment for the growth of single-walled materials in the interior of CNTs, additional samples were prepared. MWCNT/PbI_2 mixtures were furnace annealed maintaining the synthesis conditions previously reported for the growth of single-walled PbI_2 within CNTs,[17] and the resulting sample was also analyzed by HAADF-STEM (Figure S7). Visual inspection of the images shows clear differences between the structures grown within MWCNTs by laser irradiation (Figure 2, Figure S2) and conventional thermal annealing (Figure S7). In the case of conventional thermal treatments there is a strong tendency towards the formation of nanowires of PbI_2 (orange arrows), observed as continuous bright bars inside the MWCNTs. On the contrary, the presence of long PbI_2 inorganic nanotubes (green arrows) covering the entire interior of CNTs was predominant when laser treatments were carried out. It is worth noting that when conventional annealing treatments are performed, metal halide nanotubes and nanorods tend to coexist in an individual CNT forming nanotube-nanorod junctions[17] and therefore, metal halide nanotubes above 35 nm in length are already considered as "long" specimens.[18] Remarkably, the majority of single-walled PbI_2 nanotubes prepared by laser irradiation have lengths of hundreds of nanometers.

HAADF-STEM analyses were performed to quantitatively determine the production yield of single-walled PbI_2 nanotubes. The yield turned out to be more than four times higher when using

laser irradiation (ca. 94 % of filled CNTs contained PbI_2 nanotubes; 80 $mJ \cdot cm^{-2}$ fluence and 1000 pulses) compared to conventional thermal annealing (21.7 % of filled CNTs contained PbI_2 nanotubes). Similar production yields, within experimental error, were observed when employing 100 $mJ \cdot cm^{-2}$ fluence (1000 pulses). From these analyses it is clear that laser treatment leads to the selective formation of high quality single-walled PbI_2 nanotubes, their dimensions depending on the length and inner diameter of the hosting carbon nanotubes.

It should be remarked that hitherto such selective growth of inner metal halide nanotubes has not been obtained through conventional annealing treatments. Actually, using the same annealing temperature (500 ºC ± 25 ºC) a similar yield has been reported for the production of single-walled ZnI_2 inside CNTs[18] (21.4 %; mp(ZnI_2) = 446 ºC,[42] $T_{filling}$ = 475 ºC), and even for the formation of multi-walled PbI_2 and BiI_3 in the cavities of WS_2 nanotubes[45] (around 20 % of iodide nanotubes; mp(PbI_2) = 410 ºC,[42] mp(BiI_3) = 408.6 ºC,[42] $T_{filling}$ = 500 ºC). Prolonged 14-30 days of annealing were employed when using WS_2 nanotubes as templates.[45, 46] A higher amount of single-walled nanotubes within CNTs has been recently reported upon increasing the temperature of annealing, from 21.4 % at 475 ºC to 64.9 % at 1000 ºC, for the van der Waals solid ZnI_2.[18] Nevertheless, not only the production yield is still lower than the one reported here (for PbI_2 using laser) but also much longer tubular structures are obtained by laser irradiation.

Considering that the temperature employed for the synthesis of PbI_2 nanotubes by conventional annealing (500 ºC) is considerably lower than the temperature reached by laser irradiation at 80 $mJ \cdot cm^{-2}$ and 100 $mJ \cdot cm^{-2}$ (796 ºC and 953 ºC respectively, as per photothermal simulations reported in Figure 1), additional thermal treatments of MWCNT/PbI_2 pellets were carried out at these temperatures. Under these conditions the presence of inorganic nanostructures within

MWCNTs was barely observed (Figure S8). Furthermore, the few observed structures did not show selectivity towards the formation of inorganic nanotubes.

Raman spectroscopy analyses were performed to determine the quality of MWCNTs' structure after laser irradiation. Laser irradiation induces high temperature thermal cycles, which can lead to the formation of structural defects, premelting and even amorphisation of MWCNTs.[47] Raman spectra recorded on both non-irradiated and irradiated MWCNT/PbI_2 areas were fitted using four Lorentzian and one Gaussian function in the range from 1100-1700 cm^{-1} (Figure 3, Figure S9). The $I_{D''}/I_G$ ratio was calculated to account for structural variations (Table S1). Despite a slight increase in the $I_{D''}/I_G$ ratio in samples treated with fluences of 80 and 100 $mJ \cdot cm^{-2}$, this variation does not represent a significant change in the morphology and amount of structural defects of the MWCNTs. Therefore, the encapsulation of PbI_2 within the hollow core of MWCNTs is expected to take place through the open-ends rather than through structural defects on the MWCNT walls.

Mechanism of Formation of Tubular van der Waals Heterostructures. As mentioned above, the laser assisted synthesis is highly selective towards the formation of PbI_2 nanotubes with respect to PbI_2 nanowires. Furthermore, when PbI_2 nanotubes are present within the cavities of MWCNTs a 100% selectivity towards the formation of single-walled PbI_2 was observed; multi-walled PbI_2 were not detected. The reason behind the high selectivity towards the formation of monolayered PbI_2 nanotubes with respect to their multi-walled counterparts lies in the physico-chemical properties of the template employed (Elicarb® MWCNTs) rather than from the method employed for their synthesis. In the first report on the growth of PbI_2 nanotubes using the conventional thermal annealing method, the formation of multi-walled PbI_2 was also not observed.[17] In a more recent study, from over 600 inorganic metal halide nanotubes grown within MWCNTs (CeI_3, $CeCl_3$, $TbCl_3$ and ZnI_2) only in one case an inorganic nanotube bearing

more than one layer was reported (a triple-walled nanotube of ZnI_2), the rest being single-walled (*i.e.* over 99.8 % selectivity).[18] The employed MWCNTs in all these studies have internal diameters up to 9 nm, with a larger proportion of nanotubes between 4 and 6 nm.[18] A PbI_2 monolayer has a larger thickness than atomically thin van der Waals solids such as graphene. As a consequence the formation of multi-walled metal halides within the relatively small cavities of the MWCNTs employed in this study might not be favored because it would have high strain energy. In contrast, the formation of multi-walled metal halide nanotubes has been observed in the cavities of WS_2 nanotubes, which have larger diamters.[45, 46] The diameter of the host is not the only parameter that needs to be taken into account when forming tubular core-shell heterostructures. For instance, using a semi-empirical model, it was shown that PbI_2 nanotubes became stable within the core of MoS_2 nanotubes only above a critical core diameter of the host (>12 nm); below this diameter the PbI_2 was found to crystallize as nanowires.[45] These model calculations were in agreement with the experimental observations.[45] In contrast, when using CNTs as templates the formation of PbI_2 nanotubes occurs well below 12 nm.

Molten phase capillary wetting has been suggested as the growth mechanism of a large variety of metal halide nanowires inside the cavities of carbon nanotubes, using the methodology that we are referring to as "conventional thermal annealing treatment". Following this approach, PbI_2 nanowires were grown by Flahaut *et al.* inside the cavities of single-walled and double-walled carbon nanotubes back in 2006.[48] Theoretical calculations on the capillary imbibition of PbI_2 melt into inorganic and carbon nanotubes suggest that when the ionic melt wets the interior of the host nanotube forming a convex meniscus a PbI_2 nanowire will be obtained on cooling, whereas when a concave meniscus is created by capillary wetting an inorganic PbI_2 nanotube will be formed on cooling.[49]

Other mechanisms have been employed for the growth of layered metal halides. Large-scale 2D PbI_2 monolayers and few-layers have been recently grown on a SiO_2/Si substrate by a catalyst-free physical vapor deposition process.[26] In this case, PbI_2 was added to a ceramic boat and the substrate was placed on top. The furnace was then annealed to 683 K (409.85 ºC) at a rate of 24 K/min for short periods of time (1-3 min). Vapor deposition of PbI_2 onto the substrate was observed under these conditions.[26] In another study, Tenne *et al.* used electron beam irradiation of a powder of SbI_3 to create tubular core-shell structures using WS_2 as templates. Evaporation followed by recrystallization was suggested as the growth mechanism.[45]

Despite further studies are needed, we reason that the laser irradiation method might favor the vapor deposition of PbI_2 and enhance the formation of PbI_2 nanotubes, whereas capillary wetting would be predominant by the conventional thermal annealing, the latter favoring the formation of nanowires. In fact, molecular dynamic simulations reveal that insertion of molten PbI_2 into CNTs would lead to the formation of PbI_2 nanowires because a convex meniscus is obtained due to the weak wetting of the CNTs by the ionic melt.[49] Therefore an alternative growth mechanism should be proposed to justify the high yield of single-walled PbI_2 obtained by the laser process. Taking into account that vapor deposition has been employed for the growth of monolayer PbI_2 onto a SiO_2/Si substrate at ca. 410 ºC,[26] it seems plausible that the same growth mechanism takes place during laser processing. Besides, after irradiation of the MWCNT/PbI_2 pellet deposition of PbI_2 is observed on the quartz window of the vacuum chamber, indicating the presence of PbI_2 vapor during the process. Nevertheless, molten phase capillary wetting cannot be ruled out since resolidified PbI_2 is also observed in the irradiated areas. After the filling experiment using the conventional thermal annealing, the carbon nanotubes are embedded within resolidified PbI_2, indicating that the carbon nanotubes were in direct contact with the PbI_2 melt during the

annealing step. Therefore, molten phase capillary wetting seems to be favored when using this approach. As mentioned, in the conventional annealing treatment a mixture of CNTs and PbI_2 is placed on one end of a silica ampoule and vacuum-sealed. After the heating step, a slight deposition of PbI_2 is actually observed at the opposite end (cool end during the annealing), far away from the CNTs. Therefore under these experimental conditions vapor deposition would be less favored.

Optoelectronic Properties. Next, the electronic properties of the prepared materials were investigated. Local resistance characterization of PbI_2 and MWCNT/PbI_2 pellets irradiated with a laser fluence of 80 $mJ \cdot cm^{-2}$ and 1000 accumulated pulses were performed by conducting AFM (Figure 4). Resistance map histograms, presented in Figure 4A, clearly show that a non-irradiated MWCNT/PbI_2 pellet is less resistive than a pellet of PbI_2 (six orders of magnitude difference in resistance), due to the conducting nature of the MWCNTs. Both, resistance map images (a1 and a2) and corresponding histograms indicate a pronounced decrease on the resistance of the MWCNT/PbI_2 pellet (blue histogram; average resistance of 3 kΩ) after laser irradiation (red histogram; avg. resistance 1 kΩ). The non-irradiated material consists of a mixture of bulk PbI_2 and empty MWCNTs. The irradiated sample still contains a PbI_2 matrix but the MWCNTs become filled with concentric single-layers of PbI_2. Therefore, the higher conductivity observed after irradiation could arise from the formed heterostructures of PbI_2@MWCNTs. This hypothesis was confirmed by analyzing an additional control sample, prepared by irradiating a pellet of bulk PbI_2 under the same laser conditions (80 $mJ \cdot cm^{-2}$ and 1000 pulses). Conducting AFM measurements on the irradiated PbI_2 did not present such an increase in conductivity but rather revealed some fading of its resistance. This was probably

caused by the formation of larger crystals, with an obvious decrease of grain boundaries, after laser-induced melting and resolidification processes.

Lead iodide being a light sensitive material and taking into account the interest that van der Waals heterostructures of conductive (CNTs) and optically active (PbI_2) materials have for the miniaturization of devices,[20] we characterized the optoelectronic response of the material. Electrical characterization of laser irradiated MWCNT/PbI_2 was carried out through current-voltage spectroscopy loops in dark conditions and under illumination with a blue light emitting diode (LED, ca. 465 nm dominant wavelength). As it can be observed in Figure 4B, the current flowing through the material considerably increases upon illumination, accounting for significant carrier photogeneration processes. Remarkably this effect was not observed in a pellet of bulk PbI_2 where no difference in the conductivity was registered upon illumination. A schematic representation of the experimental set-up employed for the conducting AFM measurements is presented in Figure 4C. It is worth noting that despite single-walled lead iodide nanotubes are protected by the concentric graphene layers of carbon nanotubes, they remain optically active. Actually, according to Geim *et al.* each graphene layer is expected to add 2.3 % opacity,[50] therefore since the employed CNTs have an average of nine concentric graphene walls (Figure S10), about 79.3 % of incident light is expected to reach the inner cavities of the carbon nanotubes, where lead iodide is present. Based on DFT calculations a substantial enhancement of the visible light response would be expected when interfacing electrically active graphene with single-layers of PbI_2 nanosheets.[25]

Versatility of the Laser-Assisted Filling of Carbon Nanotubes. To complete the study we investigated whether it was possible to expand the laser-assisted synthesis of tubular van der Waals heterostructures to other materials. For this purpose, the same strategy that was employed

for the formation of PbI_2@MWCNTs was tested using ZnI_2 as filling material and MWCNTs as hosts. Open-ended MWCNTs were finely ground with zinc iodide powder, and a pellet of 1.3 cm in diameter and ca. 0.5 mm in thickness was prepared by applying a pressure of 10 T to the MWCNT/ZnI_2 mixture. The pellet was irradiated with an incident laser fluence of 100 $mJ \cdot cm^{-2}$ using 1000 pulses. The laser-irradiated area was gently scratched and the collected sample was deposited onto a lacey carbon support grid for TEM inspection. As it can be seen in Figure 5, HAADF-STEM imaging confirmed the successful formation of single-walled ZnI_2 nanotubes inside the cavities of MWCNT (see Figure S11 for additional images). The intensity profile acquired along the red arrow (right panel in Figure 5) is in agreement with the presence of a single-walled nanotube. The growth of inorganic nanotubes of ZnI_2 within the cavities of MWCNTs provides evidence of the versatility of the laser-assisted methodology presented herein for the synthesis of tubular van der Waals heterostructures.

CONCLUSIONS

We explored an ultrafast energy efficient methodology for the synthesis of tubular van der Waals heterostructures composed of single-walled lead iodide nanotubes along the inner walls of multi-walled carbon nanotubes. The synthetic strategy, which benefits from fast thermal cycles induced by pulsed laser irradiation, is highly selective towards the growth of single-walled lead iodide nanotubes. This contrasts to previous reports on the encapsulation of van der Waals metal halides into the cavities of CNTs where the formation of nanowires is favored by conventional thermal annealing. It is worth pointing out that whereas core-shell nanostructures of carbon and inorganic materials have been traditionally prepared by filling carbon nanotubes, more recently a complementary synthetic strategy has received widespread attention where previously

synthesized nanowires are covered by a graphene sheet.[51] The laser methodology employed here results in the formation of cylindrical van der Waals heterostructures of a conductive (CNT) and a light sensitive material (PbI_2), which conductivity can be tuned upon illumination, caused by the photogeneration of carriers. The carbon shell offers protection and stability to the monolayers of air sensitive lead iodide[26] thus allowing its manipulation under ambient conditions. Furthermore, since the single-layers of lead iodide easily accommodate to the inner diameter and shape of the CNTs, it should allow strain engineering of van der Waals solids. It is well established that the properties of single-layered crystals can be tuned by inducing strain, for instance upon bending.[6] Versatility of the laser-assisted synthesis was confirmed by growing single-walled ZnI_2 within MWCNTs. We believe that the use of laser irradiation, which is widely employed in industrial processes, will allow the encapsulation of a large variety of materials into CNTs including for the formation of van der Waals heterostructures in a simple, fast, and energy efficient manner.

METHODS

MWCNTs Purification. MWCNTs (CVD, Thomas Swan & Co. Ltd.) were firstly steam purified to remove amorphous carbon and catalyst nanoparticles, as previously reported.[52] This procedure involves placing MWCNTs in a furnace at 900 °C for 5 h with a constant flow of steam/argon mixture. Being a mild oxidizer, steam oxidizes graphitic shell around catalyst nanoparticles and opens the nanotubes' ends. Subsequently, the sample was placed into a round-bottom flask and refluxed with 6 M HCl at 110 °C for 6 h to remove the catalyst particles, cooled down and filtered through 0.2 μm polycarbonate membrane filters, washing with distilled water until neutral pH was reached and dried.

Laser-assisted Synthesis of PbI_2 Nanotubes. 36 mg of purified MWCNTs were mixed with 210 mg of PbI_2 (Strem Chemicals Inc.) and well homogenized using an agate pestle and mortar inside an argon-filled glovebox. Pellets with 1.3 cm in diameter and ca. 0.5 mm in thickness were formed applying a pressure of 10 T to the MWCNT/PbI_2 mixture. An additional pellet containing 260 mg of PbI_2 was prepared to be employed as a reference.

Pulsed laser treatments of MWCNT/PbI_2 pellets were carried out by means of a Nd:YAG laser system (266 nm, 3 ns pulse duration, 10 Hz pulse repetition rate; Brilliant model from Quantel). The experiments were performed inside a vacuum chamber at a pressure of 10-4 Pa to avoid oxidation reactions. A quartz window was placed on top of the pellet to prevent direct deposition of PbI_2 onto the optical window of the vacuum chamber. The irradiations were done by focusing the laser beam onto the sample surface, creating 1×1 mm^2 homogeneous squared spots. The distance between two adjacent irradiated spots was set to be 1 mm. Different samples were obtained by accumulation of 10, 100 and 1000 subsequent laser pulses per site with an incident laser fluence of 40, 60, 80 and 100 $mJ \cdot cm^{-2}$. Two additional samples were prepared using 10000 pulses (100 $mJ \cdot cm^{-2}$) and 200 $mJ \cdot cm^{-2}$ (1000 pulses).

Synthesis of PbI_2 Single-walled Nanotubes by Thermal Treatment. Steam purified and HCl treated MWCNTs (6 mg) and PbI_2 (140 mg) were ground together with an agate mortar in a free oxidant atmosphere and placed into a silica ampoule, evacuated and sealed under vacuum. Afterward, the sample was annealed employing a 5 ºC·min^{-1} heating rate, dwelled at 500 ºC for 12 h and cooled to room temperature. Additional samples were prepared by annealing MWCNT/PbI_2 pellets, prepared as detailed above for the laser assisted synthesis, at 796 ºC and 953 ºC.

Laser-assisted Synthesis of ZnI_2 Nanotubes. 9 mg of purified MWCNTs were mixed with 300 mg of ZnI_2 (Sigma-Aldrich) and well homogenized using an agate pestle and mortar inside an argon-filled glovebox. Pellets with 1.3 cm in diameter and ca. 0.5 mm in thickness were formed applying a pressure of 10 T to the MWCNT/ZnI_2 mixture. The pellet was irradiated as described above for PbI_2.

Sample Characterization. Spots were characterized by Raman spectroscopy (Horiba Jobin Yvon) operating at 532 nm and using 100× objective. Acquisition time was set to 30 s and laser power to 0.5 mW. Spectra were obtained from several random places at each irradiated spot and fitted using OriginPro 8 software. Scanning electron microscopy characterization was performed on an FEI Magellan 400L at 5 kV, using a through-lens (TLD) detector for secondary electrons acquisition and a vCD detector optimized for high-contrast backscattered detection at low kV. Additionally the morphology of the irradiated spots was evaluated using high-angle annular dark field (HAADF) imaging in high resolution scanning transmission electron microscopy (STEM), carried out in a FEI Tecnai G2 F20 microscope operating at 200 kV. Samples were prepared by placing dropwise onto a lacey carbon support grid the dispersion obtained after sonication of a scratched fraction of the laser-irradiated area in hexane. Films morphology and resistance at the sub-micron scale was characterized by atomic force microscopy (AFM) using a 5500LS system from Agilent Technologies equipped with a Resiscope II module (CSI Instruments). Resistance maps were acquired in contact mode using diamond-coated silicon tips with a diameter of about 100 nm. The resistance maps were acquired by applying 1 V between tip and sample. Current-voltage (I-V) spectroscopy analyses were also performed at specific locations of the samples by measuring the current flow through the tip in contact with the samples' surface while ranging the

applied voltage between -1 V and 1 V. The analysis of topographic and electric measurements was carried out with the MountainsMap 7.0 software package from Digital Surf.

Photothermal Simulation. The temperature evolution of the MWCNT-PbI_2 composite submitted to laser irradiation was modelled through a simple model composed by a carbon nanotube immersed in a matrix of PbI_2. The calculation was carried out by solving a 3D transient heat conduction model by means of partial differential equations using COMSOL Multiphysics 5.3 software. Specific details on the photothermal simulation are included in the Supporting Information.

FIGURES

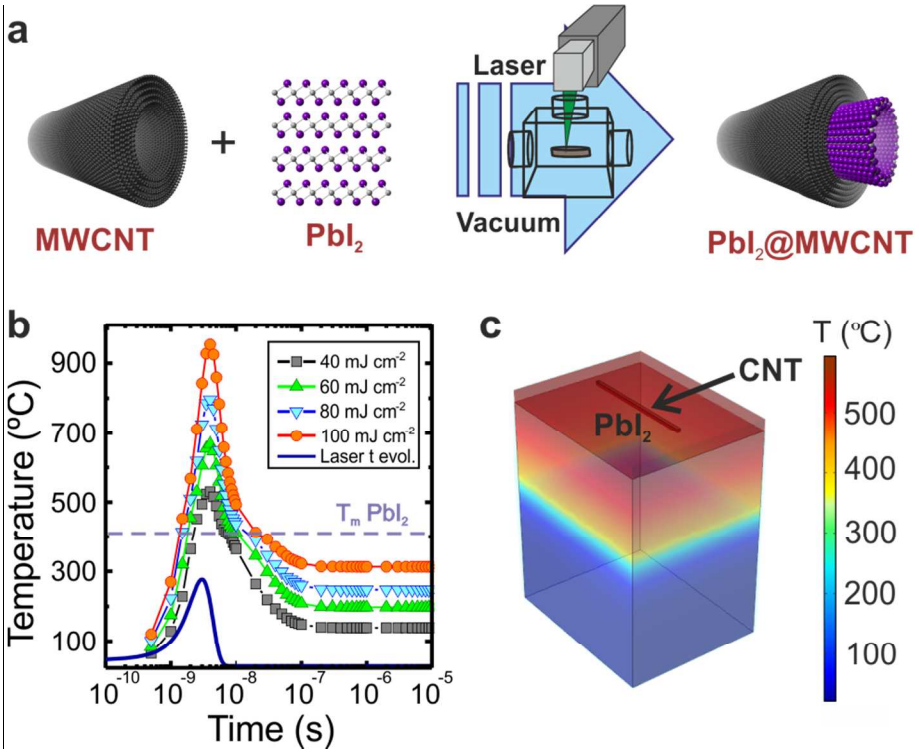

Figure 1. Laser-assisted filling of carbon nanotubes and photothermal simulation of the irradiated PbI_2/MWCNT pellet. (a) Schematic representation of the laser-assisted filling of multi-walled carbon nanotubes. C, Pb and I atoms are represented by black, purple and grey spheres respectively. Note that bulk PbI_2 and the MWCNT are not schematically drawn in the same scale to better appreciate the layered crystal structure of bulk PbI_2. The PbI_2/MWCNT pellet (brown) is laser irradiated (plotted in green) inside the vaccum chamber. (b) Temporal evolution of the temperature of the pellet's surface upon irradiation with different laser fluences. The time evolution of the laser intensity is plotted for reference with a blue continuous line (a. u.). (c) 3D plot of temperature distribution in the MWCNT-PbI_2 system irradiated with 60 $mJ \cdot cm^{-2}$ at 5 ns.

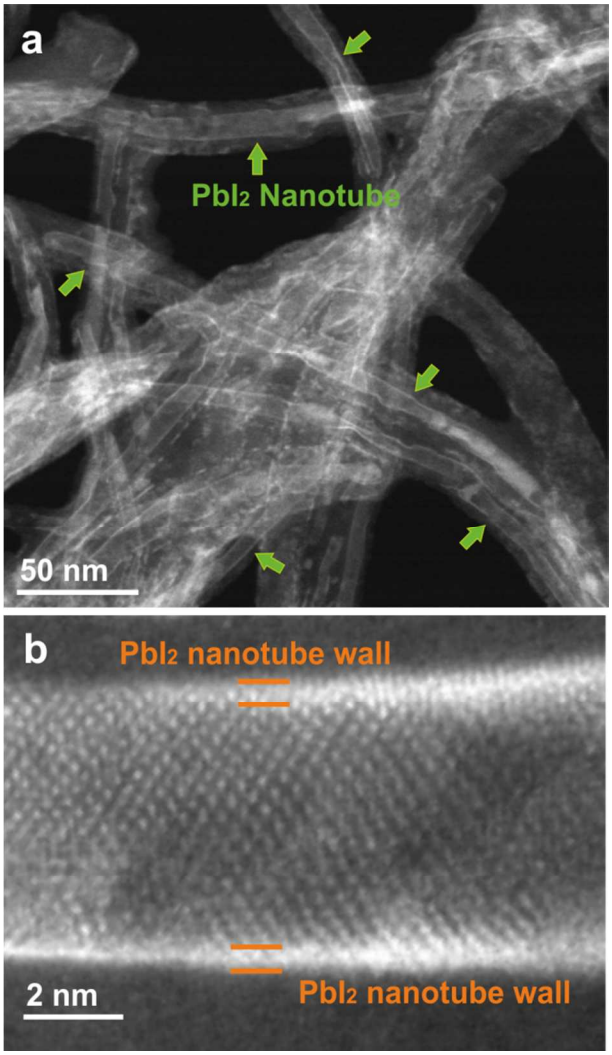

Figure 2. HAADF-STEM images of PbI_2@MWCNTs prepared by laser irradiation employing an 80 $mJ \cdot cm^{-2}$ fluence and 1000 pulses. (a) HAADF-STEM image (as prepared), (b) high resolution aberration corrected HAADF-STEM image (after one year of sample preparation). Green arrows in (a) point to well-defined single-walled inorganic PbI_2 nanotubes, while orange lines in (b) indicate the PbI_2 nanotube wall.

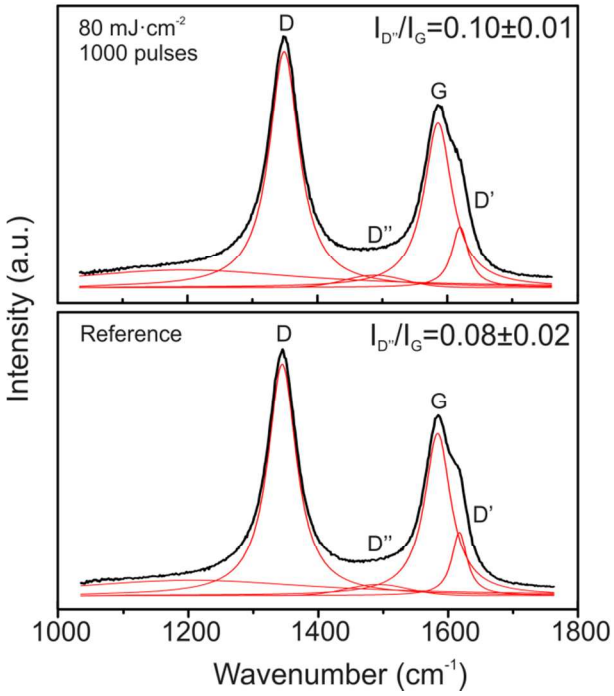

Figure 3. Deconvoluted Raman spectra acquired on PbI_2/MWCNTs after laser irradiation employing 80 $mJ \cdot cm^{-2}$ fluence and 1000 pulses and a non-irradiated area (reference). The experimental data curve and the fitting curves are shown in black and red respectively.

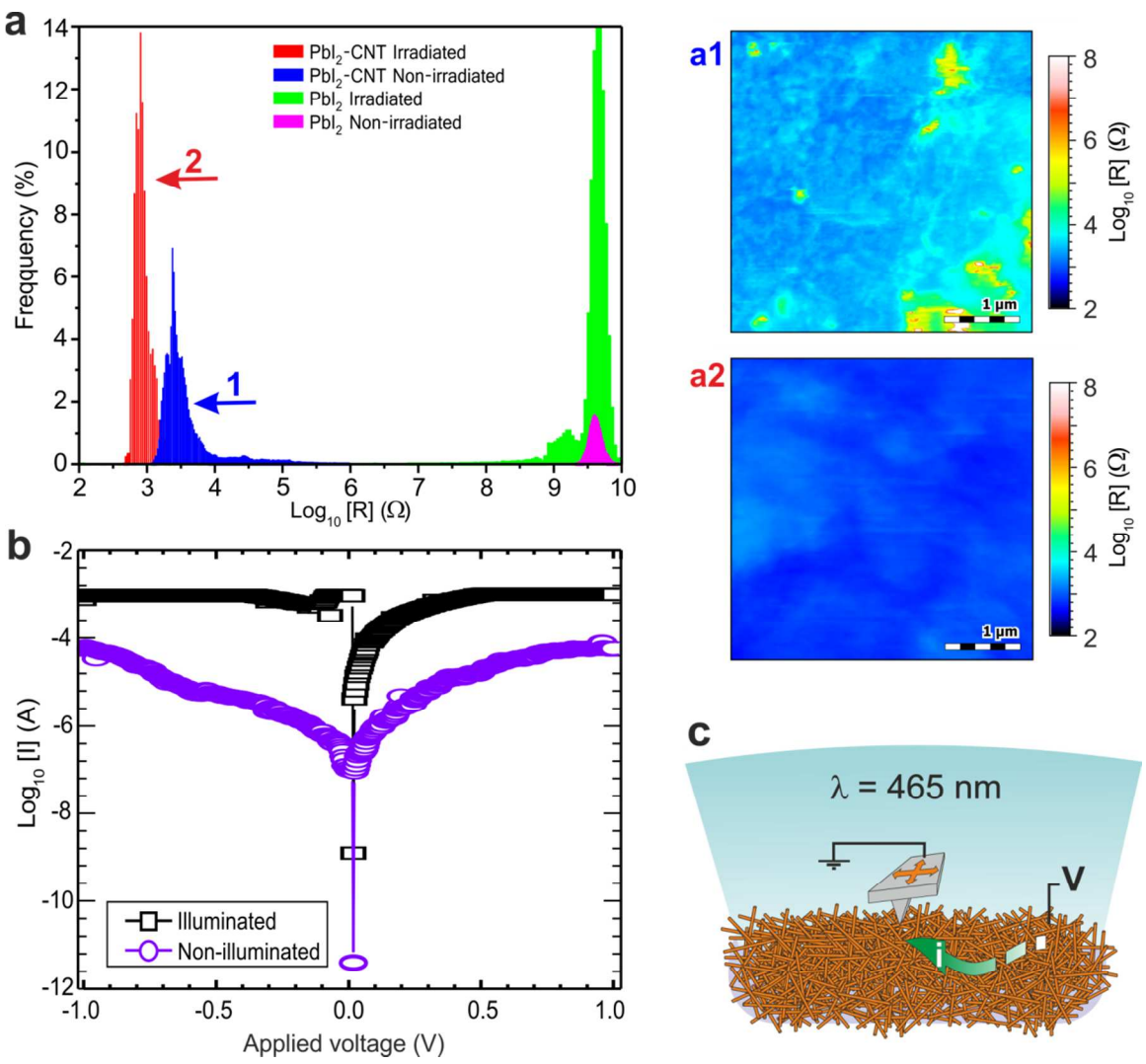

Figure 4. Conducting AFM measurements of PbI_2 and PbI_2@MWCNTs pellets before and after laser irradiation with 80 $mJ \cdot cm^{-2}$ and 1000 pulses. (a) Resistance map histograms. a1: resistance map of PbI_2@MWCNTs prior to irradiation; a2: resistance map of PbI_2@MWCNTs after irradiation. (b) Current-voltage spectroscopies of laser irradiated PbI_2@MWCNTs in dark conditions and illuminated with a blue LED (ca. 465 nm dominant wavelength). (c) Schematic representation of the experimental set-up employed for the conducting AFM measurements. Small orange cylinders represent PbI_2@MWCNTs.

Figure 5. HAADF-STEM image of ZnI_2@MWCNT prepared by laser irradiation employing 100 $mJ \cdot cm^{-2}$ fluence and 1000 pulses. The intensity profile along the red arrow is included on the right side of the image.

ACKNOWLEDGMENTS

We acknowledge funding from MINECO (Spain), through MAT2017-86616-R, ENE2017-89210-C2-1-R and "Severo Ochoa" Programme for Centres of Excellence in R&D (SEV- 2015-0496, SEV-2013-0295), CERCA programme for funding ICN2 and support from AGAUR of Generalitat de Catalunya through the projects 2017 SGR 1086, 2017 SGR 581 and 2017 SGR 327. We thank Thomas Swan Co. Ltd. for supplying MWCNT Elicarb® samples. D. Kepić acknowledges financial support from the Ministry of Education, Science and Technological Development of the Republic of Serbia for postdoctoral research. We are grateful to R. Rurali (ICMAB-CSIC) for providing the structural model of the PbI_2 nanotube employed for the schematic representation of PbI_2@MWCNT.

ASSOCIATED CONTENT

The authors declare no competing financial interest.

Supporting Information.

SEM, HAADF-STEM, stability studies and deconvoluted Raman spectra of laser irradiated PbI_2/MWCNTs. HAADF-STEM of thermally annealed PbI_2/MWCNTs. Statistical analysis of the number of MWCNTs walls. Details on the photothermal simulation. The Supporting Information is available free of charge on the ACS Publications website.

Supporting Information (PDF)

AUTHOR INFORMATION

Corresponding Authors

*E-mail: gerard.tobias@icmab.es (G. Tobias), aperez@icmab.es (A. Perez), belen.ballesteros@icn2.cat (B.Ballesteros).

Author Contributions

S. Sandoval and D. Kepić contributed equally to this work.

REFERENCES

1. Duong, D. L.; Yun, S. J.; Lee, Y. H. Van der Waals Layered Materials: Opportunities and Challenges. *ACS Nano* **2017**, *11*, 11803-11830.

2. Kelly, A. G.; Hallam, T.; Backes, C.; Harvey, A.; Esmaeily, A. S.; Godwin, I.; Coelho, J.; Nicolosi, V.; Lauth, J.; Kulkarni, A.; Kinge, S.; Siebbeles, L. D. A.; Duesberg, G. S.; Coleman, J. N. All-Printed Thin-Film Transistors from Networks of Liquid-Exfoliated Nanosheets. *Science* **2017**, *356*, 69-73.

3. Hirunpinyopas, W.; Prestat, E.; Worrall, S. D.; Haigh, S. J.; Dryfe, R. A. W.; Bissett, M. A. Desalination and Nanofiltration through Functionalized Laminar MoS_2 Membranes. *ACS Nano* **2017**, *11*, 11082-11090.

4. Zhang, C.; Anasori, B.; Seral-Ascaso, A.; Park, S.-H.; McEvoy, N.; Shmeliov, A.; Duesberg, G. S.; Coleman, J. N.; Gogotsi, Y.; Nicolosi, V. Transparent, Flexible, and Conductive 2D Titanium Carbide (Mxene) Films with High Volumetric Capacitance. *Adv. Mater.* **2017**, *29*, 1702678.

5. Lai, Z.; Chen, Y.; Tan, C.; Zhang, X.; Zhang, H. Self-Assembly of Two-Dimensional Nanosheets into One-Dimensional Nanostructures. *Chem* **2016**, *1*, 59-77.

6. Rafael, R.; Andrés, C.-G.; Emmanuele, C.; Francisco, G. Strain Engineering in Semiconducting Two-Dimensional Crystals. *J. Phys. Condens. Mat.* **2015**, *27*, 313201.

7. Hwang, D. Y.; Choi, K. H.; Park, J. E.; Suh, D. H. Highly Thermal-Stable Paramagnetism by Rolling up MoS_2 Nanosheets. *Nanoscale* **2017**, *9*, 503-508.

8. Mohammad, H. T.; Volker, J. S. Enhanced Photon Absorption in Spiral Nanostructured Solar Cells Using Layered 2D Materials. *Nanotechnology* **2015**, *26*, 344005.

9. Liu, P.; Jin, Z.; Katsukis, G.; Drahushuk, L. W.; Shimizu, S.; Shih, C.-J.; Wetzel, E. D.; Taggart-Scarff, J. K.; Qing, B.; Van Vliet, K. J.; Li, R.; Wardle, B. L.; Strano, M. S. Layered and Scrolled Nanocomposites with Aligned Semi-Infinite Graphene Inclusions at the Platelet Limit. *Science* **2016**, *353*, 364-367.

10. Gao, J.; Liu, X.; Zhang, G.; Zhang, Y.-W. Nanotube-Terminated Zigzag Edges of Phosphorene Formed by Self-Rolling Reconstruction. *Nanoscale* **2016**, *8*, 17940-17946.

11. Soto Lamata, I.; Alonso-González, P.; Hillenbrand, R.; Nikitin, A. Y. Plasmons in Cylindrical 2D Materials as a Platform for Nanophotonic Circuits. *ACS Photonics* **2015**, *2*, 280-286.

12. Rao, C. N. R.; Govindaraj, A. Synthesis of Inorganic Nanotubes. *Adv. Mater.* **2009**, *21*, 4208-4233.

13. Višić, B.; Panchakarla, L. S.; Tenne, R. Inorganic Nanotubes and Fullerene-Like Nanoparticles at the Crossroads between Solid-State Chemistry and Nanotechnology. *J. Am. Chem. Soc.* **2017**, *139*, 12865-12878.

14. Jiang, J.; Meng, Y.; Zhang, L.; Liu, M. Self-Assembled Single-Walled Metal-Helical Nanotube (M-H_n): Creation of Efficient Supramolecular Catalysts for Asymmetric Reaction. *J. Am. Chem. Soc.* **2016**, *138*, 15629-15635.

15. Liu, H.; Li, H.; Wang, X. Electrostatic Interaction-Directed Growth of Nickel Phosphate Single-Walled Nanotubes for High Performance Oxygen Evolution Reaction Catalysts. *Small* **2016**, *12*, 2969-2974.

16. Ni, B.; Liu, H.; Wang, P.-P.; He, J.; Wang, X. General Synthesis of Inorganic Single-Walled Nanotubes. *Nat. Commun.* **2015**, *6*, 8756.

17. Cabana, L.; Ballesteros, B.; Batista, E.; Magén, C.; Arenal, R.; Oró-Solé, J.; Rurali, R.; Tobias, G. Synthesis of PbI_2 Single-Layered Inorganic Nanotubes Encapsulated within Carbon Nanotubes. *Adv. Mater.* **2014**, *26*, 2016–2021.

18. Sandoval, S.; Pach, E.; Ballesteros, B.; Tobias, G. Encapsulation of Two-Dimensional Materials inside Carbon Nanotubes: Towards an Enhanced Synthesis of Single-Layered Metal Halides. *Carbon* **2017**, *123*, 129-134.

19. Toth, P. S.; Velický, M.; Bissett, M. A.; Slater, T. J. A.; Savjani, N.; Rabiu, A. K.; Rakowski, A. M.; Brent, J. R.; Haigh, S. J.; O'Brien, P.; Dryfe, R. A. W. Asymmetric MoS_2/Graphene/Metal Sandwiches: Preparation, Characterization, and Application. *Adv. Mater.* **2016**, *28*, 8256-8264.

20. Novoselov, K. S.; Mishchenko, A.; Carvalho, A.; Castro Neto, A. H. 2D Materials and van der Waals Heterostructures. *Science* **2016**, *353*, aac9439.

21. Roy, K.; Ahmed, T.; Dubey, H.; Sai, T. P.; Kashid, R.; Maliakal, S.; Hsieh, K.; Shamim, S.; Ghosh, A. Number-Resolved Single-Photon Detection with Ultralow Noise van der Waals Hybrid. *Adv. Mater.* **2018**, *30*, 1704412.

22. Roy, K.; Padmanabhan, M.; Goswami, S.; Sai, T. P.; Ramalingam, G.; Raghavan, S.; Ghosh, A. Graphene-MoS_2 Hybrid Structures for Multifunctional Photoresponsive Memory Devices. *Nat. Nanotechnol.* **2013**, *8*, 826-830.

23. Chaudhary, S. K. Lead Iodide Crystals as Imput Material for Radiation Detectors. *Cryst. Struct. Theor. App.* **2012**, *1*, 21-24.

24. Li, W.; Wang, Z.; Deschler, F.; Gao, S.; Friend, R. H.; Cheetham, A. K. Chemically Diverse and Multifunctional Hybrid Organic–Inorganic Perovskites. *Nat. Mater. Rev.* **2017**, *2*, 16099.

25. Zhou, M.; Duan, W.; Chen, Y.; Du, A. Single Layer Lead Iodide: Computational Exploration of Structural, Electronic and Optical Properties, Strain Induced Band Modulation and the Role of Spin-Orbital-Coupling. *Nanoscale* **2015**, *7*, 15168-15174.

26. Zhong, M.; Zhang, S.; Huang, L.; You, J.; Wei, Z.; Liu, X.; Li, J. Large-Scale 2D PbI_2 Monolayers: Experimental Realization and Their Indirect Band-Gap Related Properties. *Nanoscale* **2017**, *9*, 3736-3741.

27. Botos, A.; Biskupek, J.; Chamberlain, T. W.; Rance, G. A.; Stoppiello, C. T.; Sloan, J.; Liu, Z.; Suenaga, K.; Kaiser, U.; Khlobystov, A. N. Carbon Nanotubes as Electrically Active Nanoreactors for Multi-Step Inorganic Synthesis: Sequential Transformations of Molecules to Nanoclusters and Nanoclusters to Nanoribbons. *J. Am. Chem. Soc.* **2016**, *138*, 8175-8183.

28. Spencer, J. H.; Nesbitt, J. M.; Trewhitt, H.; Kashtiban, R. J.; Bell, G.; Ivanov, V. G.; Faulques, E.; Sloan, J.; Smith, D. C. Raman Spectroscopy of Optical Transitions and Vibrational Energies of ~1 nm HgTe Extreme Nanowires within Single Walled Carbon Nanotubes. *ACS Nano* **2014**, *8*, 9044-9052.

29. Chamberlain, T. W.; Biskupek, J.; Skowron, S. T.; Markevich, A. V.; Kurasch, S.; Reimer, O.; Walker, K. E.; Rance, G. A.; Feng, X.; Müllen, K.; Turchanin, A.; Lebedeva, M. A.; Majouga, A. G.; Nenajdenko, V. G.; Kaiser, U.; Besley, E.; Khlobystov, A. N. Stop-Frame

Filming and Discovery of Reactions at the Single-Molecule Level by Transmission Electron Microscopy. *ACS Nano* **2017**, *11*, 2509-2520.

30. Meyer, R. R.; Sloan, J.; Dunin-Borkowski, R. E.; Kirkland, A. I.; Novotny, M. C.; Bailey, S. R.; Hutchison, J. L.; Green, M. L. H. Discrete Atom Imaging of One-Dimensional Crystals Formed within Single-Walled Carbon Nanotubes. *Science* **2000**, *289*, 1324-1326.

31. Cambré, S.; Santos, S. M.; Wenseleers, W.; Nugraha, A. R. T.; Saito, R.; Cognet, L.; Lounis, B. Luminescence Properties of Individual Empty and Water-Filled Single-Walled Carbon Nanotubes. *ACS Nano* **2012**, *6*, 2649-2655.

32. Chaban, V. V.; Prezhdo, V. V.; Prezhdo, O. V. Confinement by Carbon Nanotubes Drastically Alters the Boiling and Critical Behavior of Water Droplets. *ACS Nano* **2012**, *6*, 2766-2773.

33. Agrawal, K. V.; Shimizu, S.; Drahushuk, L. W.; Kilcoyne, D.; Strano, M. S. Observation of Extreme Phase Transition Temperatures of Water Confined inside Isolated Carbon Nanotubes. *Nat. Nanotechnol.* **2016**, *12*, 267.

34. Sloan, J.; Matthewman, G.; Dyer-Smith, C.; Sung, A. Y.; Liu, Z.; Suenaga, K.; Kirkland, A. I.; Flahaut, E. Direct Imaging of the Structure, Relaxation, and Sterically Constrained Motion of Encapsulated Tungsten Polyoxometalate Lindqvist Ions within Carbon Nanotubes. *ACS Nano* **2008**, *2*, 966-976.

35. Khlobystov, A. N. Carbon Nanotubes: From Nano Test Tube to Nano-Reactor. *ACS Nano* **2011**, *5*, 9306-9312.

36. Liu, X.; Marangon, I.; Melinte, G.; Wilhelm, C.; Ménard-Moyon, C.; Pichon, B. P.; Ersen, O.; Aubertin, K.; Baaziz, W.; Pham-Huu, C.; Bégin-Colin, S.; Bianco, A.; Gazeau, F.; Bégin, D. Design of Covalently Functionalized Carbon Nanotubes Filled with Metal Oxide

Nanoparticles for Imaging, Therapy, and Magnetic Manipulation. *ACS Nano* **2014**, *8*, 11290-11304.

37. Stoppiello, C. T.; Biskupek, J.; Li, Z. Y.; Rance, G. A.; Botos, A.; Fogarty, R. M.; Bourne, R. A.; Yuan, J.; Lovelock, K. R. J.; Thompson, P.; Fay, M. W.; Kaiser, U.; Chamberlain, T. W.; Khlobystov, A. N. A One-Pot-One-Reactant Synthesis of Platinum Compounds at the Nanoscale. *Nanoscale* **2017**, *9*, 14385-14394.

38. Wang, Z.; Li, H.; Liu, Z.; Shi, Z.; Lu, J.; Suenaga, K.; Joung, S. K.; Okazaki, T.; Gu, Z.; Zhou, J.; Gao, Z.; Li, G.; Sanvito, S.; Wang, E.; Iijima, S. Mixed Low-Dimensional Nanomaterial: 2D Ultranarrow MoS_2 Inorganic Nanoribbons Encapsulated in Quasi-1D Carbon Nanotubes. *J. Am. Chem. Soc.* **2010**, *132*, 13840-13847.

39. Sloan, J.; Kirkland, A. I.; Hutchison, J. L.; Green, M. L. H. Integral Atomic Layer Architectures of 1D Crystals Inserted into Single Walled Carbon Nanotubes. *Chem. Commun.* **2002**, 1319-1332.

40. Eliseev, A. A.; Verbitskiy, N. I.; Volykhov, A. A.; Fedorov, A. V.; Vilkov, O. Y.; Verbitskiy, I. I.; Brzhezinskaya, M. M.; Kiselev, N. A.; Yashina, L. V. The Impact of Dimensionality and Stoichiometry of CuBr on Its Coupling to sp^2-Carbon. *Carbon* **2016**, *99*, 619-623.

41. Ilie, A.; Bendall, J. S.; Nagaoka, K.; Egger, S.; Nakayama, T.; Crampin, S. Encapsulated Inorganic Nanostructures: A Route to Sizable Modulated, Noncovalent, on-Tube Potentials in Carbon Nanotubes. *ACS Nano* **2011**, *5*, 2559-2569.

42. Handbook of Chemistry and Physics. 84^{th} ed.; CRC Press: 2003-2004.

43. Nellist, P. D.; Pennycook, S. J. Direct Imaging of the Atomic Configuration of Ultradispersed Catalysts. *Science* **1996**, *274*, 413-415.

44. Palosz, B. The Structure of PbI_2 Polytypes 2H and 4H: A Study of the 2H-4H Transition. *J. Phys.: Condens. Matter* **1990**, *2*, 5285.

45. Kreizman, R.; Enyashin, A. N.; Deepak, F. L.; Albu-Yaron, A.; Popovitz-Biro, R.; Seifert, G.; Tenne, R. Synthesis of Core–Shell Inorganic Nanotubes. *Adv. Funct. Mater.* **2010**, *20*, 2459-2468.

46. Kreizman, R.; Hong, S. Y.; Sloan, J.; Popovitz-Biro, R.; Albu-Yaron, A.; Tobias, G.; Ballesteros, B.; Davis, B. G.; Green, M. L. H.; Tenne, R. Core–Shell PbI_2@WS_2 Inorganic Nanotubes from Capillary Wetting. *Angew. Chem. Int. Ed.* **2009**, *48*, 1230-1233.

47. Pérez del Pino, Á.; György, E.; Cabana, L.; Ballesteros, B.; Tobias, G. Ultraviolet Pulsed Laser Irradiation of Multi-Walled Carbon Nanotubes in Nitrogen Atmosphere. *J. Appl. Phys.* **2014**, *115*, 093501.

48. Flahaut, E.; Sloan, J.; Friedrichs, S.; Kirkland, A. I.; Coleman, K. S.; Williams, V. C.; Hanson, N.; Hutchison, J. L.; Green, M. L. H. Crystallization of 2H and 4H PbI_2 in Carbon Nanotubes of Varying Diameters and Morphologies. *Chem. Mater.* **2006**, *18*, 2059-2069.

49. Enyashin, A. N.; Kreizman, R.; Seifert, G. Capillary Imbibition of PbI_2 Melt by Inorganic and Carbon Nanotubes. *J. Phys. Chem. C* **2009**, *113*, 13664-13669.

50. Nair, R. R.; Blake, P.; Grigorenko, A. N.; Novoselov, K. S.; Booth, T. J.; Stauber, T.; Peres, N. M. R.; Geim, A. K. Fine Structure Constant Defines Visual Transparency of Graphene. *Science* **2008**, *320*, 1308-1308.

51. Dou, L.; Cui, F.; Yu, Y.; Khanarian, G.; Eaton, S. W.; Yang, Q.; Resasco, J.; Schildknecht, C.; Schierle-Arndt, K.; Yang, P. Solution-Processed Copper/Reduced-Graphene-Oxide Core/Shell Nanowire Transparent Conductors. *ACS Nano* **2016**, *10*, 2600-2606.

52. Cabana, L.; Ke, X.; Kepić, D.; Oro-Solé, J.; Tobías-Rossell, E.; Van Tendeloo, G.; Tobias, G. The Role of Steam Treatment on the Structure, Purity and Length Distribution of Multi-Walled Carbon Nanotubes. *Carbon* **2015**, *93*, 1059-1067.

TABLE OF CONTENTS